Benign-Salt/DES Processing of Papyrus to Ultralight Nanocellulose Sponges for Organic-Solvent Removal

Nithinart C. Juntadech
Rajamangala University of Technology Thanyaburi
Khathapon Pinpatthanapong
Rajamangala University of Technology Thanyaburi
Nattaya Ruengprach
Rajamangala University of Technology Thanyaburi
Phattaramat Thiamngoen
Rajamangala University of Technology Suvarnabhumi
Pitiporn Manokhoon
Rajamangala University of Technology Suvarnabhumi
Sarawut Jitpinit
Rajamangala University of Technology Thanyaburi
Thirawat Mueansichai
Rajamangala University of Technology Thanyaburi
Thaneeya Rangseesuriyachai
thaneeya.r@en.rmutt.ac.th
Rajamangala University of Technology Thanyaburi

Research Article

Keywords: Cyperus papyrus, nanocellulose, toluene, deep eutectic solvent (DES), organic solvent adsorption

Posted Date: December 12th, 2025

DOI: https://doi.org/10.21203/rs.3.rs-7780603/v1

Additional Declarations: No competing interests reported.

Benign-Salt/DES Processing of Papyrus to Ultralight Nanocellulose Sponges for Organic-Solvent Removal

Nithinart C. Juntadech[1], Khathapon Pinpatthanapong[2], Nattaya Ruengprach[2], Phattaramat Thiamngoen[3], Pitiporn Manokhoon[3], Sarawut Jitpinit[4], Thirawat Mueansichai[4] and Thaneeya Rangseesuriyachai[2*]

[1]Department of Textile Engineering, Faculty of Engineering, Rajamangala University of Technology Thanyaburi, Pathum Thani, 12110, Thailand

[2]Department of Civil Engineering, Faculty of Engineering, Rajamangala University of Technology Thanyaburi, Pathum Thani, 12110, Thailand

[3]Faculty of Engineering and Architecture, Rajamangala University of Technology Suvarnabhumi, Nonthaburi, 11000, Thailand

[4]Department of Chemical and Materials Engineering, Faculty of Engineering, Rajamangala University of Technology Thanyaburi, Pathum Thani, 12110, Thailand

Corresponding author: Thaneeya Rangseesuriyachai (e-mail: thaneeya.r@en.rmutt.ac.th)

Abstract

Hydrophobic organic solvents in pharmaceutical operations are difficult to remove due to phase immiscibility and volatility, prompting the use of biodegradable sorbents with rapid absorption and clean regeneration. This study produces papyrus (*Cyperus papyrus* L.) into nanocellulose (NC) and then creates lightweight, freeze-dried sponges for solvent capture. The objective was to establish an eco-efficient, scalable pathway and evaluate sorption performance under controlled conditions while clarifying structure–performance relationships. Papyrus was processed using sodium chloride (NaCl)-assisted hydrothermal processing (HTP), alkaline pulping, and deep eutectic solvent extraction (DES), subsequently being formed into sponges through freeze-drying. Sorption was evaluated in neat toluene as a model hydrophobic solvent utilizing sealed containers and an evaporation-adjusted mass balance. The unmodified with 1% nanocellulose sponge (NC_1.0) exhibited the highest capacity (18.22 g/g) and maintained 16.31 and 16.21 g/g in cycles 2–3 (<10% loss) under simple thermal regeneration, indicating practical reusability. Iron oxide nanoparticles (Fe_3O_4) and methyltrimethoxysilane (MTMS)-modified (NC_1.0_S) exhibited reduced capacity (8.39 g/g), consistent with Scanning electron microscopy (SEM) and energy dispersive X-ray spectroscopy (EDS) evidence of partial pore occlusion and densification after silanization. Notably, the best-performing sponge requires no hydrophobization, supporting a low-additive, low-footprint design suitable for circular wastewater management.

Keywords: Cyperus papyrus; nanocellulose; toluene; deep eutectic solvent (DES); organic solvent adsorption

Graphical Abstract

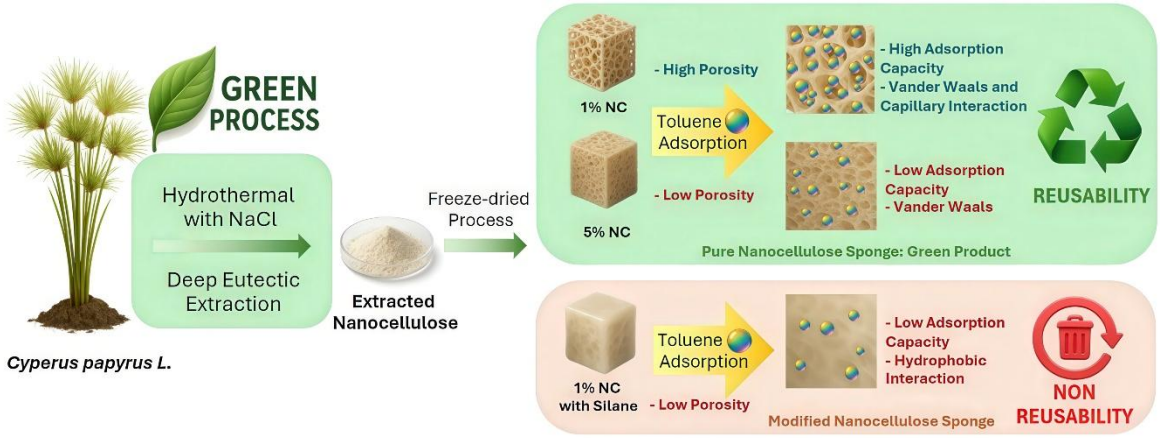

Highlights

- Benign-salt/DES processing converts papyrus into ultralight nanocellulose sponges.
- The best-performing sponge requires no hydrophobization, reducing chemicals and simplifying end-of-life.
- Rapid, reusable uptake is achieved in neat toluene (18.22 g g^{-1}; <10% loss over three cycles).
- A clear design rule emerges: pore connectivity outweighs surface silanization for solvent capture.

1. Introduction

In the pharmaceutical sector, manufacturing and downstream handling generate wastewater enriched with hydrophobic organic solvents such as toluene, dichloromethane, and benzene that are poorly miscible with water. Solvent-intensive syntheses can consume on the order of 10–800 kg of solvent per kg of active ingredient, amplifying the risk of solvent carry-over to effluents and the overall material footprint (Aboagye et al. 2021; Priya and Philip 2015). These compounds are toxic and persistent, and their control is central to green-chemistry and sustainability metrics in the pharmaceutical sector (Becker et al. 2022; Sheldon 2018). Beyond plant-level compliance, solvent losses drive life cycle impacts and Scope-3 emissions, undermining circular-economy objectives and the Sustainable Development Goals on clean water, responsible production, and climate action. Heightened regulatory scrutiny together with rising costs for solvent acquisition, recovery, and disposal sharpens the need for inexpensive, compact sorbents that operate under immiscible conditions without introducing

secondary contamination. Against these constraints, green sorbent design favors benign chemistry, minimal additives, and easy regeneration.

Conventional wet-chemistry and membrane operations (e.g., air stripping, advanced oxidation, coagulation–flotation, pressure-driven separations) can be reagent- or energy-intensive (Castel and Favre 2018; Valluri and Kawatra 2021). They often underperform for immiscible or emulsified solvent phases. These limitations motivate sorbent-based approaches that prioritise fast uptake, clean regeneration, and minimal secondary pollution (Abidli et al. 2020; Uzunok and Sonmez 2023). Bio-derived cellulose presents an advantageous substrate for sustainable sorbents: it is plentiful, lightweight, biodegradable, and may be transformed into ultralight aerogels or foams featuring linked porosity and capillary-driven absorption. Recent reviews highlight cellulose-based aerogels and nanocellulose composites exhibiting significant oil/solvent sorption capacities with simple reuse, while highlighting design levers spanning pore architecture and surface chemistry (Laitinen et al. 2017). Nanocellulose (NC), derived from various plant sources, has gained attention for its high surface area, porosity, lightweight nature, and biodegradability, making it a versatile material for various applications, including adsorption (Pandey et al. 2023).

NC is typically produced from lignocellulosic biomass via sequential pretreatment, purification, and nanofibrillation. Eco-friendly options such as hydrothermal pretreatment (HTP) and enzymatic routes are increasingly favored over harsh acid/alkali processes. HTP is known to relocate/modify lignin and thereby improve cellulose accessibility, while enzyme-based pathways reduce severity at the expense of longer processing times (Wang et al. 2022). Deep eutectic solvents (DES) alone or combined with mild mechanical/ultrasonic steps offer greener fractionation that enhances accessibility and can yield nanocellulose efficiently (Chen et al., 2019; Ma et al., 2019). Feedstock flexibility spans agricultural residues, wood, and grasses, with conditions tailored to composition (Gupta and Shukla, 2020). The main nanocellulose forms: cellulose nanofibrils (CNF), cellulose nanocrystals (CNC), and related lignin-containing grades, are distinguished by morphology and applications; abundant surface –OH groups enable silylation/esterification and other functionalizations for composites, hydrogels, and advanced materials (Trache et al. 2020). Greener pretreatment/extraction methods are reshaping process choices, while feedstock and functionalization strategies remain the key levers for tuning properties and performance.

Papyrus (*Cyperus papyrus* L.) is an abundant, under-utilized lignocellulosic resource whose conversion to NC could couple waste valorization with environmental remediation. Although papyrus-based cellulose has been studied for other applications such as for flexible electronics (Tanguy and Le Lagadec 2023), conservation

85 treatments (Ahmed et al. 2022), or heavy metal adsorption (Madivoli et al. 2016). Its deployment as a freeze-
86 dried NC sponge for organic solvent/oil adsorption has, to our knowledge, not been reported, leaving a gap in
87 sorbent design for solvent-rich industrial streams. Addressing this gap could enable biodegradable sorbents that
88 avoid the end-of-life concerns associated with many synthetic foams and carbonaceous materials.
89 The study employs toluene as a model hydrophobic solvent to delineate its properties, with sorption
90 evaluated in the pure organic phase to ensure safe handling, controlled conditions, and alignment with existing
91 literature. Papyrus-derived nanocellulose (NC) sponges are introduced as biodegradable sorbents for organic-
92 solvent removal. An eco-friendly, scalable route NaCl-assisted hydrothermal pretreatment, alkaline pulping, and
93 DES extraction aligns with circular wastewater-management principles. The study investigates absorption and
94 reusability. This work contributes to the advancement of green materials and supports multiple Sustainable
95 Development Goals (SDGs), particularly in clean water, responsible production, and climate action.
96
97 **2. Materials and methods**
98 2.1 Sample preparation and nanocellulose procedure
99 The methodology for producing nanocellulose from Cyperus papyrus L. involved several key steps,
100 beginning with the preparation of raw material. The papyrus culms were first cut into small segments
101 approximately 1-2 cm in length. These segments were then dried at a temperature of 50 °C for 24 h to a constant
102 weight. Following drying, the material was finely ground and sieved through a 100-mesh screen to achieve particle
103 sizes smaller than 0.149 mm. The chemical composition of the untreated papyrus, including cellulose,
104 hemicellulose, and lignin content, was analyzed. The remaining material was stored in airtight plastic bags for
105 further experimentation. The prepared papyrus was subjected to a hydrothermal pretreatment (HTP) process
106 combined with NaCl. The dried plant material was subjected to a NaCl-assisted hydrothermal pretreatment (HTP)
107 at various solid-to-liquor ratios (S: L = 1:30, 1:20, 1:10, 1:5; w/v) with concentrations of 1M, 2M, and 3M. The
108 treatment was conducted for 20 min at 200 °C. This treatment aimed to remove hemicellulose and lignin. After
109 the pretreatment, the papyrus was rinsed with distilled water (DI) and subsequently dried at 50 °C for 24 h. The
110 best condition was selected for further steps of nanocellulose production.
111 Subsequently, the pulping process commenced by boiling the materials at 60°C in a solution containing
112 4% sodium hydroxide (NaOH) and 7% hydrogen peroxide (H2O2) for 120 min. The stirring speed was set to 200
113 rpm with a material to solution ratio of 1:20. Once pulping was completed, the materials were rinsed with
114 deionized (DI) water and subsequently dried in an oven at 50 °C for 24 h. Following this, the material was prepared

for nanocellulose extraction using a deep eutectic solvent (DES). This involved immersing the material in DI water for 24 h and agitating it five times, one minute per agitation. Subsequently, it was heated in a 50% DES (Method adapted from Ma, Yue, et al. (2019) concentration (choline chloride/oxalate 1M in a 1:1 ratio) at 200 rpm. The mixture was maintained at a boiling temperature of 80 °C for 1 h, with a solid to liquid ratio of 1:25. After boiling, the mixture was allowed to cool, then centrifuged to separate the slurry, and dried for 10 h at 50 °C. The samples were then analyzed for lignin, cellulose, and hemicellulose content following the pretreatment, pulping, and DES extraction processes. The nanocellulose produced was then tested for its effectiveness in adsorbing organic solvents from pharmaceutical wastewater.

After the extraction of nanocellulose, a porous sponge was fabricated via freeze-drying. To impart magnetic functionality and enhance hydrophobicity, the nanocellulose was functionalized with iron oxide nanoparticles (Fe_3O_4) and methyltrimethoxysilane (MTMS), respectively. The nanocellulose was first dispersed in deionized (DI) water and stirred using a magnetic stirrer until a homogeneous suspension was achieved. MTMS (20 wt% in Ethanol) and Fe_3O_4 (0.1 wt%) were then added to the dispersion under continuous stirring at pH 4. The resulting mixture was poured into a silicone mold and frozen at −40 °C overnight. Freeze-drying was subsequently carried out under vacuum for 48 hours using a Labconco FreeZone Bulk Tray Dryer to obtain the final porous structure. Freeze-dried nanocellulose (NC) sponges were prepared from aqueous dispersions with cellulose mass fractions of 0.5, 1.0, 1.5, 2.0, 2.5, and 5.0 wt% (samples NC_0.5, NC_1.0, NC_1.5, NC_2.0, NC_2.5, and NC_5.0, respectively). Unless otherwise specified, these samples contained no additional modifiers. An additional variant, NC_1.0_S, was formulated at 1.0 wt% cellulose in deionized water and post-modified by silanization with MTMS (1.0 wt%) while incorporating Fe_3O_4 (0.1 wt%) as a magnetic additive.

2.2 Characterization of nanocellulose

The synthesized nanocellulose was characterized using the following techniques:

2.2.1 Attenuated total reflectance Fourier-transform infrared (ATR-FTIR): Functional group analysis of the nanocellulose samples was carried out using an attenuated total reflectance Fourier-transform infrared (ATR-FTIR) spectrometer (Nicolet iS5, Thermo Fisher Scientific, Waltham, MA, USA) operated with Omnic software. Each spectrum was collected with 64 scans at a resolution of 4 cm^{-1} using automatic signal acquisition. A background spectrum was recorded before analyzing each sample. ATR correction and consistent manual baseline adjustments were applied to all spectra to ensure data accuracy.

2.2.2 X-ray Diffraction (XRD): XRD analysis was conducted to determine the crystalline structure and crystallinity index of the nanocellulose samples. The measurements were carried out using a Rigaku TTRAX III diffractometer equipped with Cu Kα radiation (λ = 1.5406 Å), operating at 40 kV and 40 mA. The diffraction patterns were recorded over a 2θ range of 5° to 90° with a step size of 0.02°. The crystalline index (CrI) was calculated using the Segal method, based on the intensity of the crystalline peak I_{002} and the minimum intensity of the amorphous background (I_{am}) (Segal et al. 1959).

2.2.3 Transmission Electron Microscopy (TEM): TEM was employed to observe the morphology and size distribution of the nanocellulose. The samples were prepared by dispersing the nanocellulose in deionized water, followed by sonication for 10 minutes to ensure uniform dispersion. A small drop of the suspension was placed onto a carbon-coated copper grid and dried under vacuum at room temperature. Imaging was conducted using a JEOL JEM-2100 (JEOL Ltd., Japan) at an accelerating voltage of 200 kV with a magnification of 20,000x. TEM images were used to analyze fiber morphology and estimate nanocellulose dimensions.

2.2.4 Scanning Electron Microscopy and Energy Dispersive X-ray Spectroscopy (SEM/EDS): SEM was employed to observe the surface morphology and porous structure of the freeze-dried nanocellulose samples. Prior to imaging, the samples were mounted onto aluminum stubs using carbon adhesive tape and sputter-coated with a thin layer of gold to enhance conductivity. SEM imaging was conducted using a (SEM model: JSM-5410LV, JEOL) operated at an accelerating voltage of 20 kV. Elemental composition of the samples was analyzed using EDS attached to the SEM system. EDS analysis was performed to confirm the presence of elements introduced during the modification process, such as silicon (Si) from MTMS and iron (Fe) from Fe_3O_4. Elemental mapping and point analysis were conducted to evaluate the distribution and relative abundance of these elements within the sample matrix.

2.3 Organic oil adsorption test

The adsorption capacity of nanocellulose for organic oil from pharmaceutical wastewater was evaluated using batch adsorption experiments. In the experiment to evaluate the oil absorption efficiency, freeze-dried nanocellulose samples according to the detail in Section 2.1, were first cut into approximately 1 cm x 1 cm x 0.5 cm and their initial weights were measured. The samples were then immersed in neat toluene 5 mL, and removed from the oil after 3 min, respectively. Immediately after removal, the samples were weighed to calculate the oil adsorption capacity. The data were analyzed and presented as a comparative graph illustrating the average oil adsorption capacities of the three sample groups. Error bars representing standard deviation were included to indicate variability within each group. After the test, the samples were placed in an oven at 110 °C for 5 min to

evaporate the oil. The cleaned samples were then subjected to three cycles of repeated oil absorption tests. The data collected was analyzed to assess the oil adsorption efficiency and the stability of the nanocellulose material for potential reuse. Tests were performed in sealed glass vials using neat toluene as the model solvent; capacities are reported as mean ± SD (n = 3) using an evaporation-corrected mass balance.

3. Results and discussion

3.1 Chemical composition of papyrus after pretreatment process

Papyrus is predominantly composed of cellulose, hemicellulose, and lignin, with minor constituents including ash, proteins, and lipids. The structural components are essential in assessing the material's appropriateness for nanocellulose manufacturing. Prior to any pretreatment, the chemical composition of papyrus in this study was determined to be 34.45% cellulose, 8.41% hemicellulose, 25.80% lignin, and 31.34% others. The increased lignin percentage emphasizes the necessity for an effective pretreatment approach to improve cellulose purity for later applications. Comparisons with previous research, including Sheferaw et al. (2023), demonstrate essentially consistent results, with minor variations likely attributable to differences in culture conditions, plant age, and growth habitat. The experimental results show that the composition of papyrus fibers changes significantly after a hydrothermal pretreatment HTP with NaCl at varied ratios and concentrations as shown in Fig. 1.

The chemical composition of papyrus was significantly altered following HTP with NaCl at different concentrations and treatment ratios. The effectiveness of the pretreatment process was evaluated based on the enhancement of cellulose purity and the reduction of hemicellulose and lignin content. Among different treatment ratios, the 1:20 and 1:30 ratios exhibited superior performance in cellulose enhancement and non-cellulosic removal. While 1:30 with 3M NaCl achieved 40.16% cellulose, it retained slightly higher lignin (13.42%) compared to 1:20 with 3M NaCl (40.18% cellulose, 8.47% lignin), making the 1:20 ratio the optimal condition for achieving high-purity cellulose. Conversely, at a lower 1:5 ratio, even with 3M NaCl, the maximum cellulose content achieved was 38.05%, with 9.81% lignin remaining. This suggests that reduced treatment ratios are less helpful in destroying lignocellulosic structures, resulting in insufficient lignin extraction. This tendency is similar across all treatment ratios (1:5, 1:10, 1:20, and 1:30), with 3M NaCl consistently yielding the maximum cellulose content while reducing hemicellulose and lignin levels. The results indicate that elevated NaCl concentrations, together with suitable pretreatment ratios, markedly enhance cellulose purity by efficiently eliminating

considerable quantities of hemicellulose and lignin. Thus, HTP processing with NaCl demonstrates efficacy in removing papyrus fibers, improving their appropriateness for nanocellulose production.

The compositional study following hydrothermal pretreatment (HTP) with NaCl demonstrates that this technique effectively disrupted the lignocellulosic structure of papyrus, leading to an increased cellulose content and diminished amounts of hemicellulose and lignin. This modification can be mechanistically elucidated by the ability of chloride ions (Cl^-) to infiltrate the fiber matrix and disrupt hydrogen bonds between lignin and hemicellulose, thereby augmenting the porosity of the structure and providing a more sustainable and economical approach, utilizing NaCl (Thiamngoen et al. 2022).

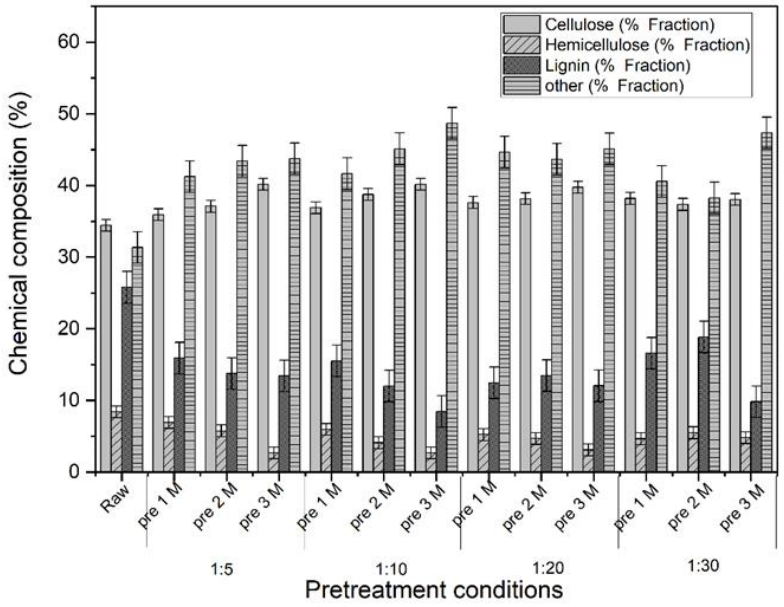

Fig. 1 Composition of papyrus after hydrothermal pretreatment combined with NaCl at various treatment ratios and concentrations.

3.2 Chemical composition of papyrus after nanocellulose extraction

Despite the analysis results showing that a solid-to-liquor ratio (S:L) of 1:20 at 3 M NaCl yielded elevated cellulose content with no residual lignin, downstream processing factors preferred a solid-to-liquor ratio (S:L) of 1:10 at 3 M NaCl for further experimentation. Augmenting the solids loading (diminishing fluid volume) reduced the bath volume and drying load, decreased handling time, and enhanced sponge formability without jeopardizing the desired cellulose purity within experimental margins of error. From a process-intensification standpoint, the

1:10, 3 M condition signifies a more scalable operating point that reconciles composition objectives with throughput, solvent consumption, and energy requirements. After the pretreatment process, pretreated papyrus was pulped by using a papyrus-to-solution ratio of 1:10, 3M. Following pulping, the material was subjected to nanocellulose extraction with a deep eutectic solvent (DES). Stage-wise composition and yields (Table 1) corroborate effective hemicellulose/lignin removal during pretreatment–pulping, with a DES-stage rebound in hemicellulose fraction but high cellulose yield.

The progressive chemical changes observed during the four processing steps demonstrate the efficiency of each step in increasing cellulose purity while reducing hemicellulose and lignin levels. The most significant changes happened during pretreatment and pulping, when hemicellulose and lignin were substantially decreased, resulting in increased cellulose concentration. This outcome is consistent with recent research on lignocellulosic biomass processing, which have indicated that alkaline and hydrothermal treatments disrupt lignin-carbohydrate connections, promoting hemicellulose dissolution and partial delignification (Awoyale and Lokhat 2021; Trajano et al. 2013). Pulping further refined the cellulose content, demonstrating a synergistic effect with the pretreatment step. The additional reduction in hemicellulose and lignin confirms that pulping enhances fiber purification. The alkaline environment provided by NaOH helped solubilize hemicellulose, while the oxidative action of H_2O_2 selectively degraded lignin without excessively degrading cellulose, converting it into oxidized carbonyl and carboxyl groups (Sun et al. 2001). Stage-wise mass balances (Table 1) indicate that pretreatment removes much of the hemicellulose and a portion of lignin while retaining most cellulose. Pulping sharpens this purification, trading overall solids for higher fiber quality: cellulose retention remains high, hemicellulose yield collapses, and lignin continues to decline. The small loss of cellulose across these steps is consistent with co-extraction of fines/ash rather than substantive cellulose degradation.

Interestingly, DES extraction did not maintain the expected trend of cellulose enrichment. Instead, a minor decrease in cellulose content and a rise in hemicellulose were detected. The effectiveness of lignin removal in these conditions may be attributed to the presence of lactic acid in the DES formulations, which promotes hemicellulose hydrolysis and facilitates lignin dissolution (Li et al. 2023). The decrease in lignin content, however, indicates the selective delignification capability of DES solvents, which has been previously reported in other lignocellulosic systems (Kohli et al. 2020). This unanticipated reversal is consistent with DES-induced disruption of cellulose structure, including possible reductions in degree of polymerization and decrystallization upon dissolution–regeneration. A contribution from non-cellulosic redeposition cannot be ruled out, although direct evidence under the present DES conditions is lacking and warrants further study (Chen et al. 2019). Deep eutectic

solvents (DESs) are effective delignification media that enhance cellulose accessibility; they can also solubilize and partially hydrolyze hemicellulose, depending on solvent composition and severity. A contribution from re-precipitation or re-adsorption of dissolved hemicellulose during regeneration/washing is plausible when polarity conditions change, though direct evidence under the present conditions remains limited (Thulluri et al. 2021; Yao et al. 2024). The rise in solid recovery and hemicellulose yield alongside modest lignin decrease is consistent with partial re-adsorption/re-precipitation of solubilized hemicellulosic species during DES regeneration/washing and/or carry-over/uptake of DES components, which would elevate apparent mass and dilute cellulose percentage without truly compromising cellulose retention. This reconciles the higher cellulose yield with a lower cellulose percentage at the DES stage.

Table 1 Stage-wise composition and component yields of papyrus during nanocellulose production (dry basis).

Stage no.	Condition	Solid recovery (%)	Cellulose (%)	Hemicellulose (%)	Lignin (%)	Cellulose yield (%)	Hemicellulose yield (%)	Lignin removal (%)
1	Raw	100.00	34.45	8.41	25.80	100.00	100.00	100.00
2	Pretreatment	82.64	39.77	3.09	10.79	90.26	56.87	52.14
3	Pulping	70.00	41.06	1.80	10.13	86.90	12.88	26.32
4	DES extraction	86.07	39.23	4.02	7.67	93.27	61.71	28.18

Note: Solid recovery (%) = (mass (stage)/mass (raw)) ×100

Cellulose/hemicellulose/lignin yield (%) = (component mass(stage)/component mass(raw))×100

Lignin removal (%) = 100−100-100− lignin yield

3.3 Characterization of nanocellulose

3.3.1 Transmission Electron Microscopy

Nanocellulose was extracted from papyrus using a DES composed of choline chloride and oxalic acid and subsequently analyzed by transmission electron microscopy (TEM) to investigate its nanoscale morphology. Prior to the DES treatment, the raw material was soaked in distilled water for 24 h and subjected to several spinning cycles to promote fiber dispersion and disrupt weak intermolecular interactions. The DES process was carried out at 80 °C and 200 rpm for 1 h, effectively breaking the lignin and hemicellulose linkages, thereby releasing cellulose nanostructures. TEM analysis (Fig. 2) revealed a well-developed fibrillar network consisting of elongated, entangled nanofibers with uniform diameter distribution. The fibers exhibited minimal aggregation and good dispersion, indicating that the DES treatment efficiently deconstructed the lignocellulosic matrix while preserving the nanofibrillar architecture. The observed fiber diameters, ranging from approximately 10 to 50 nm, confirm the successful production of cellulose nanofibrils (CNFs) from papyrus.

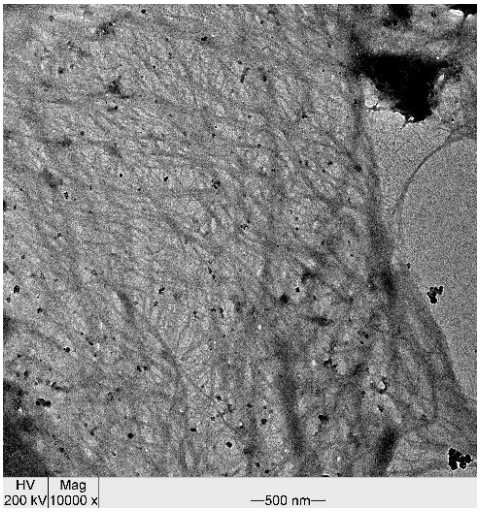

Fig. 2 TEM image of nanocellulose extracted from papyrus using a DES, showing well-dispersed nanofibrils (10–50 nm).

3.3.2. X-ray diffraction crystallinity analysis

Structural evolution during processing was assessed by X-ray diffraction (XRD), with crystallinity index (CrI) values reported for each stage below. The diffraction profiles of the samples at various stages raw, pretreated, pulped, and DES-extracted nanocellulose are presented in Supplementary (Fig. S1). The results show a progressive increase in structural order across the processing sequence. The raw lignocellulosic sample displays broad, low-intensity reflections with a notable feature at ~2θ ≈ 22°, assigned to the (002) plane of cellulose I; its low crystallinity index (CrI = 25.58%) indicates a predominantly amorphous matrix, consistent with residual lignin and hemicellulose that disrupt native chain packing. Following hydrothermal pretreatment in 3 M NaCl at 200 °C, the diffraction peaks become narrower and more intense, and the CrI rises to 35.91%, suggesting partial removal of amorphous domains and improved chain organization, likely aided by NaCl-induced fiber swelling and partial hemicellulose solubilization. Subsequent chemical pulping with $NaOH/H_2O_2$ further sharpens the reflections and yields the highest CrI (40.80%), confirming efficient delignification/ dehemicellulosation and the reorientation of cellulose microfibrils into a more compact crystalline arrangement. Finally, extraction using DES produces well-defined cellulose peaks with a CrI of 35.97%, indicating preservation of crystalline regions alongside removal of amorphous components. Although slightly lower in CrI than the pulped sample, the DES-based extraction process appears effective in producing nanocellulose with a high degree of structural order.

3.3.3 Fourier Transform Infrared Spectroscopy analysis

The chemical structure changes of papyrus through various pretreatment processes were studied using FTIR techniques to investigate the chemical structure and functional groups. The FTIR spectra of different samples are presented in Supplementary (Fig. S2), where distinct peaks corresponding to various functional groups can be observed.

The raw material exhibits characteristic peaks corresponding to cellulose, hemicellulose, and lignin. A broad absorption band at 3335 cm^{-1} (Hinterstoisser et al. 2001), attributed to O–H stretching vibrations, indicates the presence of hydroxyl groups in cellulose and bound water. This peak remains visible throughout the treatment process, though its intensity increases after deep eutectic solvent (DES) treatment, suggesting enhanced hydrogen bonding and a more organized cellulose structure. The range of 1765–1715 cm^{-1} indicated the C=O group from the glucosidic bonds of hemicellulose. The range of 1,300–1,000 cm^{-1} highlighted C–O–C stretching in polysaccharides (cellulose/hemicellulose) (Nikonenko et al. 2000).

The C–H stretching peak at 2900 cm^{-1} (Hinterstoisser et al. 2001), assigned to aliphatic C–H stretching in polysaccharides and residual lignin, gradually diminishes following hydrothermal pretreatment and pulping,

indicating progressive removal of non-cellulosic components. The absorption band significantly reduced, reinforcing the notion of cellulose purification. The absorption band at 1729 cm^{-1} (Lionetto et al. 2012), attributed to the C=O stretching vibrations of ester and carbonyl groups primarily from hemicellulose, undergoes a marked reduction after pretreatment, suggesting partial hemicellulose removal. This peak continues to decrease with pulping process and is completely absent in the final stage, confirming the total elimination of hemicellulose. Similarly, the peaks at 1630 cm^{-1} (Hinterstoisser et al. 2001) and 1427 cm^{-1} (Comnea-Stancu et al. 2017), associated with the C=C stretching of aromatic rings in lignin, exhibit a stepwise decline as the treatment progresses. with the ~1030 cm^{-1} band (C–O stretching) becoming the dominant feature, consistent with progressive removal of non-cellulosics and cellulose enrichment.

From the FTIR analysis, it was found that each pretreatment step reduced lignin and hemicellulose components while increasing the purity and clarity of the cellulose structure. Particularly after bleaching and DES extraction, functional groups associated with cellulose, such as C-O-C (1,300–1,000 cm^{-1}), became increasingly evident following the order of pretreatment. The peak at 2115 cm^{-1} in the FTIR spectra of lignocellulosic samples is generally not an intrinsic cellulose functional group. Rather, it is commonly assigned to the water 'bending + libration' combination band (H–O–H bending coupled with libration), which appears around 2100–2130 cm^{-1} and is sensitive to absorbed/adsorbed moisture in cellulose fibers or on humid sample surfaces (Verma et al. 2018).

Comparative study of FTIR spectra exposes different levels of treatment efficiency. While cellulose stayed placed in the matrix, HTP somewhat disturbed lignin and eliminated hemicellulose. Although some residual non-cellulosic components remained, pulping with $NaOH/H_2O_2$ further broke lignin and hemicellulose, hence increasing cellulose exposure. The decrease of lignin-related peaks and the increase of cellulose-specific bands indicate that the nanocellulose synthesized after DES showed the most refined structure with the highest purity.

3.3.4 Structural analysis of freeze-dried nanocellulose samples using SEM/EDS

As shown in Fig. 3, the structural and pore morphologies of selected freeze-dried samples NC_1.0, NC_5.0, and NC_1.0_S were examined using Scanning Electron Microscopy (SEM). The NC_1.0 sample (1% nanocellulose) exhibited a highly porous structure with a well-defined, interconnected network, suggesting a relatively higher surface area compared to the NC_5.0 sample (5% nanocellulose), which displayed a denser and more compact morphology. This difference is likely attributed to the increased solid content in NC_5.0, which

may hinder pore formation during the freeze-drying process due to reduced ice crystal growth and limited phase separation.

In contrast, the NC_1.0_S sample, which was modified with silane (MTMS), showed a notably less porous and more compact structure. This reduction in porosity is likely a result of the formation of a silane cross-linked network on the nanocellulose surface, which can lead to partial pore collapse or blockage during freeze-drying. The hydrophobic silane coating may also reduce the water content and affect ice templating, further contributing to the decrease in porosity. This effect of silane modification is also consistent with previous findings reported in the literature, where surface functionalization was shown to reduce porosity due to pore blockage or structural densification (Meeks et al. 2010).

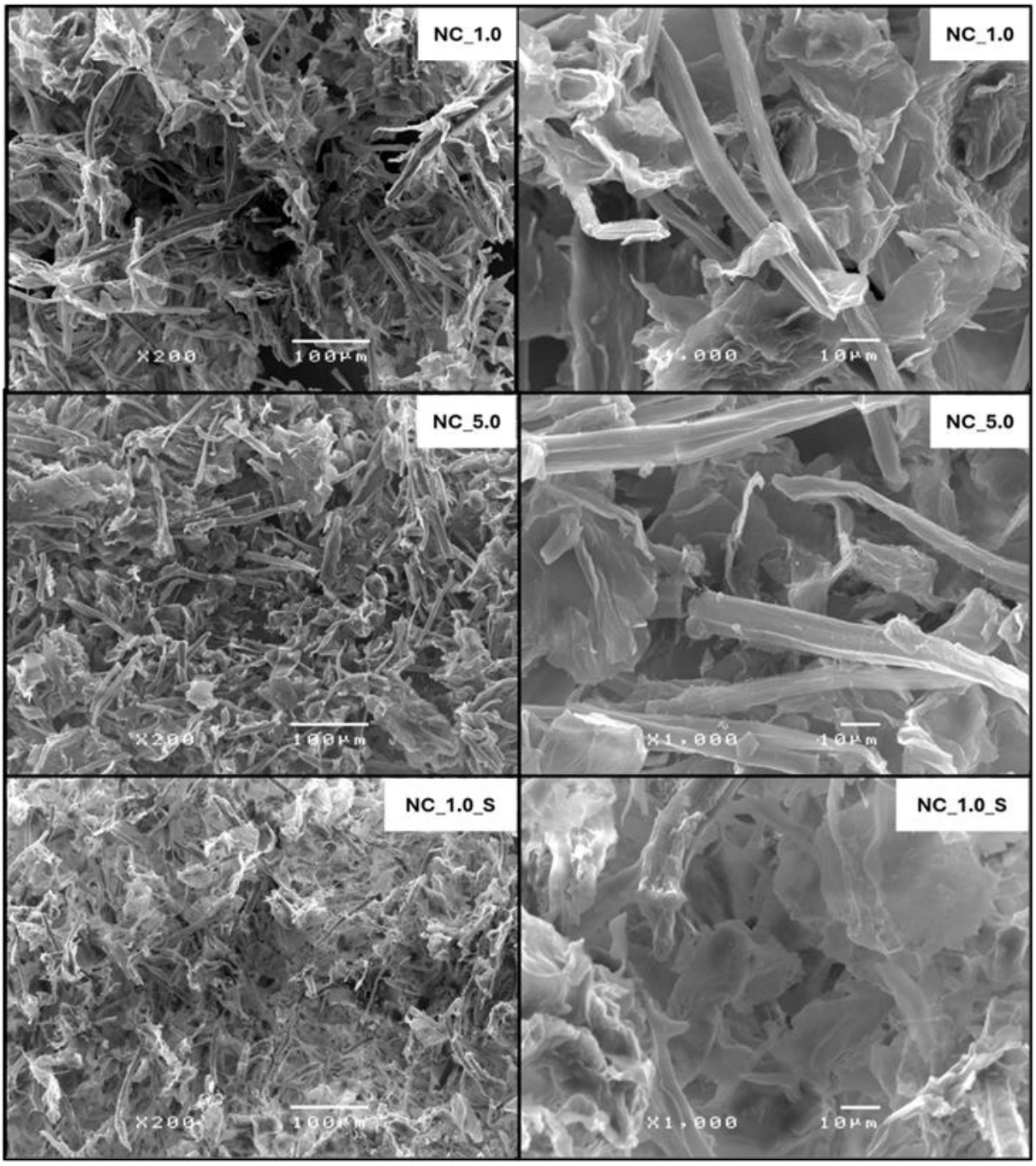

Fig. 3 SEM images of freeze-dried samples

Based on Fig. 4, the EDS spectrum and elemental mapping of the NC_1.0_S sample confirm the successful incorporation of both silane and Fe_3O_4 into the nanocellulose matrix. The presence of silicon (21.10 wt%) indicates effective surface modification with methyltrimethoxysilane (MTMS), while the detection of iron (2.51 wt%) confirms the addition of Fe_3O_4. Elemental maps show a uniform distribution of silicon and a dispersed presence of iron across the structure. The relatively low Fe content and its scattered distribution may

explain the weak magnetic response observed. The SEM image also reveals a compact morphology, consistent with the reduced porosity caused by silane crosslinking, which may limit adsorption performance.

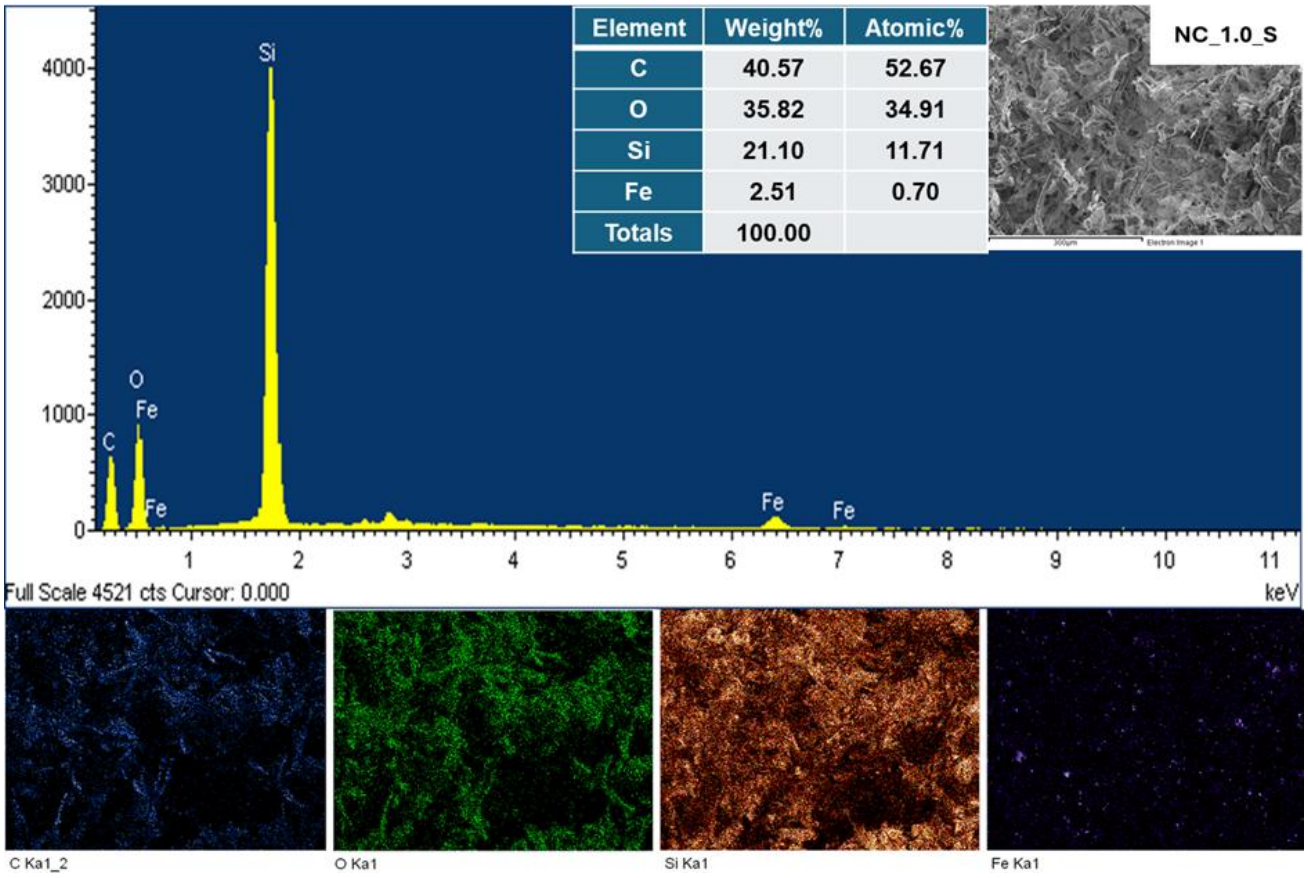

Fig. 4 EDS elemental mapping of the freeze-dried nanocellulose sample (NC_0.1_S).

3.4 Organic oil adsorption test

Nanocellulose extracted from papyrus was surface modified using methoxymethylsilane (MTMS) to enhance its hydrophobicity for the adsorption of organic oils. Additionally, iron oxide (Fe_3O_4) powder was incorporated to impart magnetic properties to the material. After shaping the samples via freeze-drying, it was observed that the unmodified nanocellulose exhibited a fluffy, highly porous structure. In contrast, the MTMS-modified samples showed denser and more compact morphology as shown in SEM images (Fig. 3). Interestingly, the Fe_3O_4-loaded samples did not exhibit any significant magnetic response. This may be attributed to an insufficient Fe_3O_4 content, particle aggregation, or the oxidation of Fe_3O_4 to non-magnetic Fe_2O_3 during processing. Such oxidation has been previously reported to diminish magnetic properties due to structural defects and phase transformation in iron oxide nanoparticles (Wetterskog et al. 2013).

In accordance with the investigation of toluene adsorption capacity of cellulose nanofibers (NC) derived from Egyptian papyrus, the NC_1.0 sample exhibited the highest toluene adsorption capacity in the initial cycle, with a value of 18.22 g/g. In contrast, the NC_1.0_S sample, which underwent surface modification with MTMS (Methyltrimethoxysilane), demonstrated the lowest adsorption capacity, recorded at 8.39 g/g (as shown in Fig. 5). As hypothesized, surface functionalization with silane was expected to introduce functional groups that could enhance the adsorption of hydrophobic compounds, such as toluene, by increasing the material's hydrophobicity (Ojogbo et al. 2025). However, as observed in the SEM images and supported by previous studies, surface modification with silane can, in some cases, adversely affect the surface area of the adsorbent. This is likely due to the formation of a silane-derived functional network, which may lead to pore blockage or structural densification, thereby reducing the available surface area (Meeks et al. 2010). In addition, the adsorption of toluene onto cellulose nanofibers is primarily facilitated by van der Waals interactions between the aromatic ring of toluene and the glucopyranose backbone of cellulose, along with capillary condensation within the porous structure (Ji et al. 2023, Cao et al. 2023). Once toluene molecules penetrate the pores, they tend to become confined and partially retained due to pore–wall interactions and physical trapping, which explains the incomplete desorption observed in subsequent cycles. In the case of silane-modified samples, the presence of –Si–CH_3 groups increases the hydrophobic affinity toward toluene, resulting in stronger binding and further limiting the reversibility of adsorption. This proposed adsorption mechanism is illustrated in Fig. 6.

Subsequent toluene adsorption tests conducted during the 2nd and 3rd cycles revealed a minor and statistically insignificant decrease in adsorption capacity across all samples. Notably, the NC_1.0 sample retained the highest adsorption capacity, with values of 16.31 g/g and 16.21 g/g for the 2nd and 3rd cycles, respectively, representing a reduction of 10.48% and 9.22% relative to the 1st and 2nd cycles. However, the NC_1.0_S sample, which was silane-modified, exhibited a significant decrease in adsorption capacity, with a reduction of 41.23% from the initial cycle. This can likely be attributed to the hydrophobic silane surface layer, which may have more tightly bound the toluene molecules after the first adsorption–desorption cycle, thereby hindering desorption in subsequent cycles. Furthermore, toluene desorption is influenced by multiple factors, including the structural integrity and pore configuration of the adsorbent material (Chen et al., 2020). This highlights that both morphological changes and molecular-level interactions between cellulose and toluene contribute to the overall adsorption–desorption behavior.

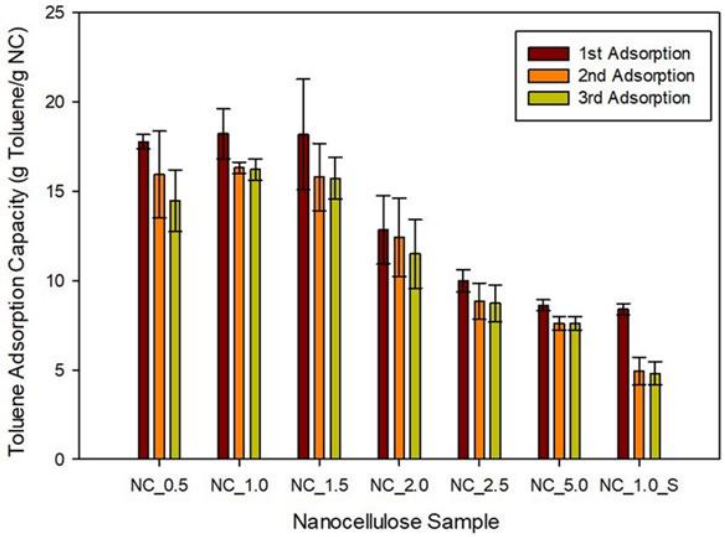

404

405 Fig. 5 Toluene adsorption capacity for each cycle.

406

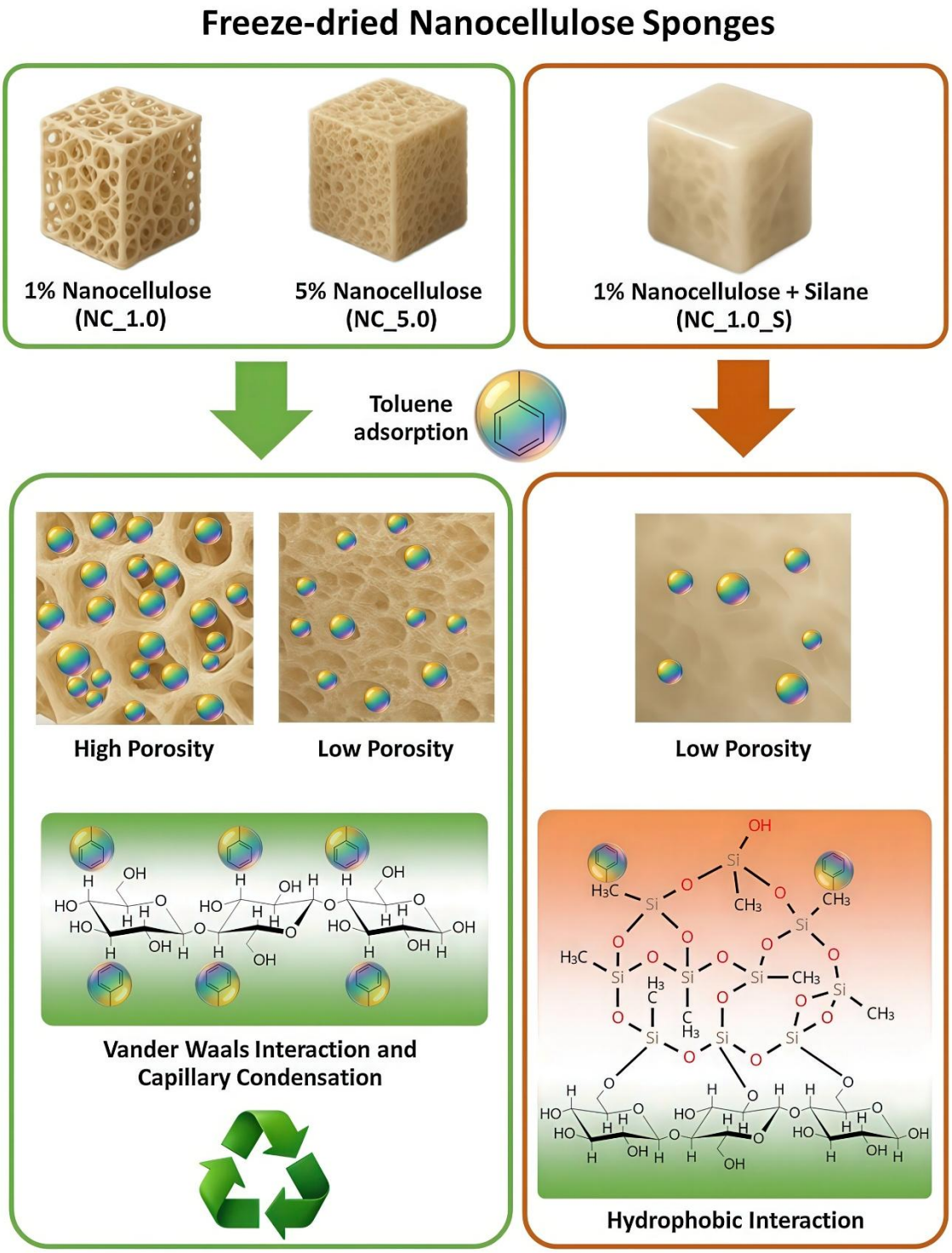

Fig. 6 Schematic illustration of the proposed interaction mechanism between toluene molecules and freeze-dried nanocellulose sponges.

To contextualize the measured capacities, a literature benchmarking was compiled for cellulose-based sponges/aerogels tested with oils or organic solvents. Table 2 positions the papyrus-derived NC sponge (neat

toluene, 18.22 g/g; three-cycle retention <10% loss) against representative cellulose-only and modified/hybrid systems reported under comparable batch protocols. Across the survey, unmodified cellulose aerogels typically report 18–25 g/g for oils/solvents, whereas aggressively hydrophobized or hybridized scaffolds span approximately 50–200 g/g depending on liquid and protocol. The papyrus-derived NC sponge falls at the upper end of unmodified cellulose systems while retaining multi-cycle performance, reinforcing the design view that pore connectivity and low bulk density are primary levers for rapid, reusable uptake.

Table 2 Benchmarking of oil/solvent uptake for cellulose-based sponges/aerogels

Sorbent / Feedstock	Surface treatment / Additives	Test liquid	Sorption capacity (g/g)	Reusability (cycles)	Notes	Reference
Papyrus-derived NC sponge (this work, NC_1.0)	None	Toluene	18.22	3 (16.31→ 16.21)	Freeze-dried NC; best performer unmodified	This work
Paper-waste cellulose aerogel	None (cellulosic aerogel)	Crude oil	24.4	NR	Early cellulose aerogel benchmark	Nguyen et al. 2013
rGO–CNC hybrid aerogel (waste-paper cellulose fibers)	rGO hybrid; ASTM F726-17	Toluene	59	NR	Measured under ASTM F726-17	Shadkam et al. 2021
Silylated CNF sponge	MTMS/alkylsilane	Marine diesel	143	NR	Very high capacity after silanization	Laitinen et al. 2017
Reed-based cellulose aerogel (Phragmites australis)	Cross-linked cellulose aerogel	Crude oil	52.3	NR	Optimized via RSM (RP aerogel)	Thi Thanh et al. 2025
Cellulose aerogel (various plant sources)	Hydrophobized (review synthesis)	Multiple oils/solvents	22–55	up to multi-cycle	Review reporting typical ranges	Long et al. 2018
Cellulose aerogel composites (paper/cardboard + wool, straw, algae, CA)	Various	Diesel / crude	32	up to 10	Range illustrations spread in literature	Paulauskienė et al. 2021
Si–CNF/BTCA aerogel	Silica + BTCA	Olive oil, gasoline, toluene	77–226	NR	Reported range across liquids	Shang et al. 2021

NR = not reported.

Note: Capacities are reported as measured under each study's protocol; direct comparisons should consider differences in test conditions (e.g., contact time, temperature, and evaporation control).

4. Conclusion

This study establishes an eco-lean route to valorize papyrus into nanocellulose and ultralight freeze-dried sponges for rapid capture of hydrophobic solvents. Sequential NaCl-assisted hydrothermal pretreatment, alkaline pulping and DES extraction yielded purified cellulose with higher crystallinity and nanofibrils (approximately 10–50 nm), enabling open, interconnected pore networks. The unmodified NC_1.0 sponge achieved the highest toluene uptake (18.22 g/g) and retained performance over three cycles (16.31→16.21 g/g) under simple thermal regeneration (<10% loss). MTMS-modified NC_1.0_S showed markedly lower capacity (8.39 g/g), consistent with SEM/EDS evidence of partial pore occlusion and densification. Findings support a green design rule for bio-cellulosic sorbents: open, interconnected porosity and low bulk density outweigh aggressive hydrophobization for rapid, reusable capture. Future research must measure bulk density, porosity, and wetting behavior, benchmark longer cycling with evaporation correction, and evaluate actual or surrogate effluents (free oil and emulsions) to enhance the case for adoption.

Acknowledgements

This research was supported by the National Science, Research and Innovation Fund, Thailand Science Research and Innovation (TSRI), through Rajamangala University of Technology Thanyaburi (FRB67E0718) (Grant No.: FRB670027/0168). The authors gratefully acknowledge the Faculty of Engineering, Rajamangala University of Technology Thanyaburi (RMUTT) for access to laboratory and pilot facilities. We thank the technical staff for their excellent assistance. Finally, we declare that there is no conflict of interest.

References

Abidli A, Huang Y, Park CB (2020) In situ oils/organic solvents cleanup and recovery using advanced oil-water separation system. Chemosphere 260:127586. https://doi.org/10.1016/j.chemosphere.2020.127586

Aboagye EA et al (2021) Systems-level roadmap for solvent recovery and reuse in the pharmaceutical industry. Cell Rep Phys Sci 24(10): 103114.

Ahmed RH, Wahba WN, Abouzeid RE, Ali KA (2022) Evaluation of starch and cellulose based consolidation materials on the mechanical properties of papyrus. Cellul Chem Technol 56:391–401.

456 Awoyale A, Lokhat D (2021) Experimental determination of the effects of pretreatment on selected Nigerian
457 lignocellulosic biomass in bioethanol production. Sci Rep 11(1): 557. https://doi.org/10.1038/s41598-
458 020-78105-8
459 Becker J et al (2022) Green chemistry and sustainability metrics in the pharmaceutical industry. Curr Opin
460 Green Sustain Chem 33: 100562. https://doi.org/10.1016/j.cogsc.2021.100562
461 Cao B, Wang C, Zhou Z (2023) Insights into the interactions between cellulose and biological molecules.
462 Carbohydr Res 523:108738.
463 Castel C, Favre E (2018) Membrane separations and energy efficiency. J Membr Sci 548:345–357.
464 https://doi.org/10.1016/j.memsci.2017.11.035
465 Chen J, Sun C, Huang Z, Qin F, Xu H, Shen W (2020) Fabrication of functionalized porous silica nanocapsules
466 with a hollow structure for high performance of toluene adsorption–desorption. ACS Omega
467 5(11):5805–5814.
468 Chen Y, Zhang X, You T, Xu F (2019) Deep eutectic solvents (DESs) for cellulose dissolution: a mini-review.
469 Cellulose 26:205–213. https://doi.org/10.1007/s10570-018-2130-7
470 Comnea-Stancu IR, Wieland K, Ramer G, Schwaighofer A, Lendl B (2017) On the identification of
471 rayon/viscose as a major fraction of microplastics in the marine environment: Discrimination between
472 natural and manmade cellulosic fibers using Fourier transform infrared spectroscopy. Appl Spectrosc
473 71(5):939–950. https://doi.org/10.1177/0003702816660725
474 Gupta GK, Shukla P (2020) Lignocellulosic biomass for the synthesis of nanocellulose and its eco-friendly
475 advanced applications. Front Chem 8:601256. https://doi.org/10.3389/fchem.2020.601256
476 Hinterstoisser B, Åkerholm M, Salmén L (2001) Effect of fiber orientation in dynamic FTIR study on native
477 cellulose. Carbohydr Res 334(1):27–37. https://doi.org/10.1016/S0008-6215(01)00167-7
478 Ji SH, Yun JS (2023) Natural cellulose-based multifunctional nanofibers for the effective removal of particulate
479 matter and volatile organic compounds. Nanomaterials 13(11):1720.
480 https://doi.org/10.3390/nano13111720
481 Kohli K, Katuwal S, Biswas A, Sharma B (2020) Effective delignification of lignocellulosic biomass by
482 microwave assisted deep eutectic solvents. Bioresour Technol 303:122897.
483 https://doi.org/10.1016/j.biortech.2020.122897
484 Laitinen O, Suopajärvi T, Österberg M, Liimatainen H (2017) Hydrophobic, superabsorbing aerogels from

485 choline chloride-based deep eutectic solvent pretreated and silylated cellulose nanofibrils for selective
486 oil removal. ACS Appl Mater Interfaces 9(29):25029–25037. https://doi.org/10.1021/acsami.7b06304
487 Li P, Zhang Z, Zhang X, Li K, Jin Y, Wu W (2023) DES: their effect on lignin and recycling performance. RSC
488 Adv 13(5):3241–3254.
489 Lionetto F, Del Sole R, Cannoletta D, Vasapollo G, Maffezzoli A (2012) Monitoring wood degradation during
490 weathering by cellulose crystallinity. Materials 5(10):1910–1922. https://doi.org/10.3390/ma5101910
491 Long LY, Weng YX, Wang YZ (2018) Cellulose aerogels: Synthesis, applications, and prospects. Polymers
492 10:623. https://doi.org/10.3390/polym10060623
493 Ma Y, Xia Q, Liu Y, Chen W, Liu S, Wang Q, Yu H (2019) Production of nanocellulose using hydrated deep
494 eutectic solvent combined with ultrasonic treatment. ACS Omega 4(5):8539–8547.
495 Madivoli ES, Kareru PG, Gachanja AN, Mugo S, Murigi MK, Kairigo P, Njonge FK (2016) Adsorption of
496 selected heavy metals on modified nano cellulose. Int Res J Pure Appl Chem 12:1–9.
497 https://doi.org/10.9734/IRJPAC/2016/28548
498 Meeks ND, Rankin S, Bhattacharyya D (2010) Sulfur-functionalization of porous silica particles and application
499 to mercury vapor sorption. Ind Eng Chem Res 49(10):4687–4693.
500 Nguyen ST, Feng J, Le NTM, Le ATT, Hoang N, Tan VBC, Duong HM (2013) Cellulose aerogel from paper
501 waste for crude oil spill cleaning. Ind Eng Chem Res 52:18386–18391.
502 https://doi.org/10.1021/ie4032567
503 Nikonenko NA, Buslov DK, Sushko NI, Zhbankov RG (2000) Investigation of stretching vibrations of
504 glycosidic linkages in disaccharides and polysaccharides with use of IR spectra deconvolution.
505 Biopolymers 57(4):257–262. https://doi.org/10.1002/1097-0282(2000)57:4<257::AID-BIP7>3.0.CO;2-
506 3
507 Ojogbo E, Tzoganakis C, Mekonnen TH (2025) Silane-modified cellulose nanocrystals (CNCs) based natural
508 rubber composites. Compos Part A Appl Sci Manuf 190:108632.
509 Pandey A, Kalamdhad A, Sharma YC (2023) Recent advances of nanocellulose as biobased adsorbent for heavy
510 metal ions removal: A sustainable approach integrating with waste management. Environ Nanotechnol
511 Monit Manag 20:100791. https://doi.org/10.1016/j.enmm.2023.100791
512 Paulauskienė T, Uebe J, Ziogas M (2021) Cellulose aerogel composites as oil sorbents and their reusability.
513 Polymers 13:2821.
514 Priya V, Philip L (2015) Treatment of volatile organic compounds in pharmaceutical wastewater using

submerged aerated biological filter. Chem Eng J 266:309–319.

Segal L, Creely J, Martin C Jr (1959) An empirical method for estimating the degree of crystallinity of native cellulose using the X-ray diffractometer. Text Res J 29(10):786–794. https://doi.org/10.1177/004051755902901003

Shadkam R, Naderi M, Ghazitabar A, Akbari S (2021) Adsorption performance of reduced graphene-oxide/cellulose nano-crystal hybrid aerogels reinforced with waste-paper extracted cellulose fibers for the removal of toluene pollution. Mater Today Commun 28:102604. https://doi.org/10.1016/j.mtcomm.2021.102604

Shang Q, Chen J, Hu Y et al (2021) Facile fabrication of superhydrophobic cross-linked nanocellulose aerogels for oil–water separation. Polymers 13:625. https://doi.org/10.3390/polym13040625

Sheferaw L, Gideon RK, Ejegu H, Gatew Y (2023) Extraction and characterization of fiber from the stem of Cyperus papyrus plant. J Nat Fibers 20(1):2149661. https://doi.org/10.1080/15440478.2023.2149661

Sheldon RA (2018) Metrics of green chemistry and sustainability : Past, Present, and Future. ACS Sustain Chem Eng 6(1): 32-48. http://dx.doi.org/10.1021/acssuschemeng.7b03505

Sun R, Tomkinson J, Mao F, Sun X (2001) Physicochemical characterization of lignins from rice straw by hydrogen peroxide treatment. J Appl Polym Sci 79:719–732. https://doi.org/10.1002/1097-4628(20010124)79:4<719::AID-APP170>3.0.CO;2-3

Tanguy NR, Le Lagadec R (2023) From papyrus to flexible electronic devices: The revolution of cellulose nanofibrils. TECNOCIENCIA Chihuahua 17(4):e1333.

Thi Thanh HL, Nguyen Minh AT, Tran Huu H (2025) Development of reed-based cellulose aerogel: a sustainable solution for crude oil spill clean-up. R Soc Open Sci 12(1):rsos.241207. https://doi.org/10.1098/rsos.241207

Thiamngoen P, Manokhoon P, Rangseesuriyachai T (2022) Application of Box–Behnken design–based response surface methodology optimization for predicting lignin residue following microwave-assisted inorganic salt (NaCl) pretreatment of Napier grass. Int J Green Energy 19(8):879–887.

Thulluri C, Balasubramaniam R, Velankar HR (2021) Generation of highly amenable cellulose-Iβ via selective delignification of rice straw using a reusable cyclic ether-assisted deep eutectic solvent system. Sci Rep 11(1):1591.

Trache D, Tarchoun AF, Derradji M, Hamidon TS, Masruchin N, Brosse N, Hussin MH (2020) Nanocellulose:

from fundamentals to advanced applications. Front Chem 8:392. https://doi.org/10.3389/fchem.2020.00392

Trajano HL, Engle NL, Foston M, Ragauskas A, Tschaplinski T, Wyman C (2013) The fate of lignin during hydrothermal pretreatment. Biotechnol Biofuels 6:110. https://doi.org/10.1186/1754-6834-6-110

Uzunok S, Sonmez HB (2023) Reusable polycaprolactone based sorbents with different cross-linking densities for the removal of organic pollutants. J Environ Chem Eng 11(2):109287. https://doi.org/10.1016/j.jece.2023.109287

Valluri S, Kawatra SK (2021) Reduced reagent regeneration energy for CO2 capture with bipolar membrane electrodialysis. Fuel Process Technol 213:106691. https://doi.org/10.1016/j.fuproc.2020.106691

Verma PK, Kundu A, Puretz MS, Dhoonmoon C, Chegwidden OS, Londergan CH, Cho M (2018) The bend+libation combination band is an intrinsic, collective, and strongly solute-dependent reporter on the hydrogen bonding network of liquid water. J Phys Chem B 122(9):2587–2599. https://doi.org/10.1021/acs.jpcb.7b09641

Wang X, Wang P, Su Y, Wang Q, Ling Z, Yong Q (2022) Supramolecular deconstruction of bamboo holocellulose via hydrothermal treatment for highly efficient enzymatic conversion at low enzyme dosage. Int J Mol Sci 23(19):11829. https://doi.org/10.3390/ijms231911829

Wetterskog E, Tai CW, Grins J, Bergstrom L, Salazar-Alvarez G (2013) Anomalous magnetic properties of nanoparticles arising from defect structures: Topotaxial oxidation of Fe1–xO/Fe3−δO4 core/shell nanocubes to single-phase particles. ACS Nano 7(8):7132–7144.

Yao Z, Chong G, Guo H (2024) Deep eutectic solvent pretreatment and green separation of lignocellulose. Appl Sci 14:7662. https://doi.org/10.3390/app14177662

Statements & Declarations

Funding

This work was supported by the National Science, Research and Innovation Fund, Thailand Science Research and Innovation (TSRI) (Grant No.: FRB670027/0168). Author Thaneeya Rangseesuriyachai has received research support through Rajamangala University of Technology Thanyaburi (FRB67E0718).

Competing Interests

The authors have no relevant financial or non-financial interests to disclose.

Author Contributions

Nithinart C. Juntadech: Conceptualization, Writing - Original Draft, Formal analysis **Khathapon Pinpatthanapong:** Data Curation, Visualization **Nattaya Ruengprach:** Formal analysis and investigation **Phattaramat Thiamngoen:** Methodology, Writing - original draft preparation **Pitiporn Manokhoon:** Resources, Investigation **Sarawut Jitpinit:** Validation, Formal analysis **Thirawat Mueansichai:** Methodology, Resources, **Thaneeya Rangseesuriyachai:** Conceptualization, Methodology, Writing- Reviewing and Editing

Supplementary Files

This is a list of supplementary files associated with this preprint. Click to download.

- FigS1.docx
- FigS2.docx